# An Anisotropic Perfectly Matched Layer-Absorbing Medium for the Truncation of FDTD Lattices

Stephen D. Gedney, *Member, IEEE*

***Abstract*—A perfectly matched layer (PML) absorbing material composed of a uniaxial anisotropic material is presented for the truncation of finite-difference time-domain (FDTD) lattices. It is shown that the uniaxial PML material formulation is mathematically equivalent to the perfectly matched layer method recently published by Berenger [2]. However, unlike Berenger's technique, the uniaxial PML absorbing medium presented in this paper is based on a Maxwellian formulation. Numerical examples demonstrate that the FDTD implementation of the uniaxial PML medium is stable, equal in effectiveness as compared to Berenger's PML medium, while being more computationally efficient.**

## I. Introduction

THE finite-difference time-domain (FDTD) method has proven to be a highly efficient technique for numerous applications in electromagnetics [1]. One of the greatest challenges of applying the FDTD technique to open radiation problems has been the development of accurate and computationally efficient absorbing boundary conditions. Very recently, the perfectly matched layer (PML) boundary condition, introduced by Berenger [2], has been used as a means to truncate FDTD lattices. The PML boundary condition is a lossy material boundary layer that is perfectly matched to the solution space. This is achieved through a "field splitting" of the electric and magnetic field intensities and the introduction of a tensor electric and magnetic conductivity, leading to a modified set of Maxwell's equations. It has been shown that an arbitrarily polarized wave incident on this PML medium is perfectly transmitted, has the same phase velocity and characteristic wave impedance as the incident wave while attenuating rapidly along the normal axis [2]–[4]. Berenger's PML method has been successfully implemented within the FDTD algorithm [2]–[7]. It has been found that the PML medium can result in reflection errors as minute as $-80$ dB to $-100$ dB [2]–[7] and can be applied to both homogeneous media [2]–[6] as well as inhomogeneous media [4], [7].

There are limitations of the present form of Berenger's PML medium, some of which are discussed in [6]. Principally, the fields within the PML medium and the governing equations are non-Maxwellian. This in itself does not detract from the usefulness of the method, however, it impedes direct physical insight into the mechanisms that render it effective. Second, the Berenger equations are based on a field splitting in a Cartesian coordinate system which results in nonstandard mathematical expressions which cannot be easily manipulated. It has been successfully mapped into locally nonorthogonal curvilinear coordinate systems [7]–[9] based on structured grids. However, the extension to unstructured grids, required by finite-element methods [10], [11] or the planar generalized Yee-algorithm [1], [12], is not obvious. Second, due to the field splitting the memory requirements and the number of floating-point operations are doubled as compared to the traditional FDTD method. Finally, it is not clear as to how to use Berenger's PML to match lossy media.

In this paper, a perfectly matched layer-boundary condition that is based on a lossy uniaxial medium is presented. Such a medium was originally suggested by Sacks *et al.* [13], [14] and has been applied to frequency-domain-based finite-element methods. It is shown that by properly choosing the parameters of the medium, the lossy uniaxial medium is "perfectly matched" to an isotropic medium. It is also shown that this formulation is physically and mathematically equivalent to the Berenger PML formulation, although it is in a form that avoids the field splitting. In the discrete space it is demonstrated that this medium can be used as a highly efficient means to terminate the FDTD lattice resulting in absorption characteristics that are equivalent to the PML. The advantage of this formulation over Berenger's PML method are: 1) the formulation is based on Maxwell's equations, rather than a modified set of equations, 2) the application to the FDTD method is more computationally efficient, and 3) it can be extended to nonorthogonal and unstructured grid techniques.

## II. Perfectly Matched Uniaxial Medium

A time-harmonic arbitrarily polarized plane wave $\vec{H}^{inc} = \vec{H}_o e^{-j\beta_x^i x - j\beta_z^i z}$ propagating in an isotropic medium is incident on a material half-space described as a uniaxial anisotropic medium. The interface between the two media is the $z = 0$ plane. The fields excited within the uniaxial medium are plane wave in nature and satisfy Maxwell's equations. In the plane-wave space the curl equations are expressed as

$$\begin{aligned} \vec{\beta}^a \times \vec{E} &= \omega\mu_o\mu_r\bar{\bar{\mu}}\vec{H} \\ \vec{\beta}^a \times \vec{H} &= -\omega\varepsilon_o\varepsilon_r\bar{\bar{\varepsilon}}\vec{E} \end{aligned} \tag{1}$$

where $\vec{\beta}^a = \hat{x}\beta_x^i + \hat{z}\beta_z^a$, $\varepsilon_r$, and $\mu_r$ are the relative permittivity and permeability of the isotropic space and

$$\begin{aligned} \bar{\bar{\varepsilon}} &= \begin{bmatrix} a & 0 & 0 \\ 0 & a & 0 \\ 0 & 0 & b \end{bmatrix} \\ \bar{\bar{\mu}} &= \begin{bmatrix} c & 0 & 0 \\ 0 & c & 0 \\ 0 & 0 & d \end{bmatrix} \end{aligned} \tag{2}$$

Manuscript received May 30, 1995; revised April 16, 1996. This work was supported in part by NSF through the Research Initiation Award ECS-9309179 and by the Army Research Office under Contract DAAH04-94-G-0243.

The author is with the Electromagnetic Laboratory, Department of Electrical Engineering, University of Kentucky, Lexington, KY 40506 USA.

Publisher Item Identifier S 0018-926X(96)08354-8.

where $\epsilon_{xx} = \epsilon_{yy}$ and $\mu_{xx} = \mu_{yy}$, since the medium is expected to be rotationally symmetric about the $z$ axis. The wave equation is then derived from the coupled curl equations

$$\vec{\beta}^a \times \overline{\overline{\varepsilon}}^{-1} \vec{\beta}^a \times \vec{H} + k^2 \overline{\overline{\mu}} \vec{H} = 0 \tag{3}$$

where $k^2 = \omega^2 \mu_o \mu_r \varepsilon_o \varepsilon_r$. Expressing the cross products as matrix operators, the wave equation can be expressed more suitably in matrix form as

$$\begin{bmatrix} k^2 c - a^{-1}\beta_z^{a^2} & 0 & \beta_x^i \beta_z^a a^{-1} \\ 0 & k^2 c - \beta_z^{a^2} a^{-1} - \beta_x^{i^2} b^{-1} & 0 \\ \beta_x^i \beta_z^a a^{-1} & 0 & k^2 d - a^{-1}\beta_x^{i^2} \end{bmatrix} \cdot \begin{bmatrix} H_x \\ H_y \\ H_z \end{bmatrix} = 0. \tag{4}$$

The dispersion relationship for the uniaxial medium is derived from the determinant of the matrix operator. Solving for $\beta_z^a$, it is found that there are four eigenmode solutions. Conveniently, these solutions can be decoupled into forward and backward $\mathrm{TE}_y$ and $\mathrm{TM}_y$ modes, which satisfy the dispersion relationships

$$\begin{cases} k^2 c - a^{-1}\beta_z^{a^2} - b^{-1}\beta_x^{i^2} = 0; & \mathrm{TE}_y \\ k^2 a - c^{-1}\beta_z^{a^2} - d^{-1}\beta_x^{i^2} = 0; & \mathrm{TM}_y. \end{cases} \tag{5}$$

The reflection coefficient at the interface of the two half-spaces can now be computed. First, assume a $\mathrm{TE}_y$ incident wave. In the upper half-space (or the isotropic space) the fields are expressed as a superposition of the incident and reflected fields

$$\begin{aligned} \vec{H}_1 &= \hat{y} H_o (1 + \Gamma e^{2j\beta_z^i z}) e^{-j\beta_x^i x - j\beta_z^i z} \\ \vec{E}_1 &= \left[ \hat{x} \frac{\beta_z^i}{\omega\varepsilon} (1 - \Gamma e^{2j\beta_z^i z}) - \hat{z} \frac{\beta_x^i}{\omega\varepsilon} (1 + \Gamma e^{2j\beta_z^i z}) \right] \\ &\quad \cdot H_o e^{-j\beta_x^i x - j\beta_z^i z}. \end{aligned} \tag{6}$$

The wave transmitted into the anisotropic half-space will also be $\mathrm{TE}_y$, with propagation characteristics governed by the dispersion relationship in (5) and is expressed as

$$\begin{aligned} \vec{H}_2 &= \hat{y} H_o \tau e^{-j\beta_x^i x - j\beta_z^a z} \\ \vec{E}_2 &= \left( \hat{x} \frac{\beta_z^a a^{-1}}{\omega\varepsilon} - \hat{z} \frac{\beta_x^i b^{-1}}{\omega\varepsilon} \right) H_o \tau e^{-j\beta_x^i x - j\beta_z^a z} \end{aligned} \tag{7}$$

where $\beta_x^a = \beta_x^i$ due to phase matching. $\Gamma$ and $\tau$ are the reflection and transmission coefficients, respectively, of the interface and are computed by enforcing the continuity of the tangential fields across the boundary interface. From (6) and (7), it is found that

$$\begin{aligned} \Gamma &= \frac{\beta_z^i - \beta_z^a a^{-1}}{\beta_z^i + \beta_z^a a^{-1}} \\ \tau &= 1 + \Gamma \\ &= \frac{2\beta_z^i}{\beta_z^i + \beta_z^a a^{-1}}. \end{aligned} \tag{8}$$

The underlying objective is to determine if there exists a choice of constitutive parameters for which $\Gamma = 0$ for all angles of incidence. To this end, it is sufficient to find under what conditions $\beta_z^i = \beta_z^a a^{-1}$. From the $\mathrm{TE}_y$ dispersion relationship in (5), this relationship can be expressed as

$$\beta_z^{i^2} = k^2 c a^{-1} - \beta_x^{i^2} b^{-1} a^{-1} \tag{9}$$

where $\beta_z^{i^2} = k^2 - \beta_x^{i^2}$. Finally, the equality in (9) is valid if $c = a$ and $b = a^{-1}$.

The above exercise is again repeated for the $\mathrm{TM}_y$ polarization. The reflection coefficient for the $\mathrm{TM}_y$ polarized wave is the dual of (8) and is found by replacing $a$ with $c$ (and vice versa) and $b$ with $d$. Subsequently, reflectionless conditions then holds if $c = a$ and $d = c^{-1}$.

In conclusion, it is found that given a plane wave incident on the uniaxial medium described in (2), if $a = c = b^{-1} = d^{-1}$, the plane wave will be purely transmitted into the uniaxial medium. Amazingly, this reflectionless property is completely independent of the angle of incidence, polarization and frequency of the incident wave. Furthermore, from (5), the propagation characteristics of the TE and TM polarized waves are identical.

For FDTD applications, this is extremely useful if the uniaxial medium is highly lossy. A wave entrant upon the medium will then quickly attenuate while no physical reflections will be encountered due to the interface. Terminating the uniaxial slab with a hard boundary such as a perfect electrical conductor (PEC), small reflections will be encountered due to the finite depth. However, if the medium is highly lossy, these reflections can be made to be extremely small.

For a lossy uniaxial medium, one obvious choice for the constitutive parameters is $a = 1 + \sigma/j\omega\varepsilon_o$. This leads to the relative permittivity and permeability tensors

$$\begin{aligned} \overline{\overline{\varepsilon}} &= \begin{bmatrix} 1 + \dfrac{\sigma}{j\omega\varepsilon_o} & 0 & 0 \\ 0 & 1 + \dfrac{\sigma}{j\omega\varepsilon_o} & 0 \\ 0 & 0 & \dfrac{1}{1 + \dfrac{\sigma}{j\omega\varepsilon_o}} \end{bmatrix} \\ &= \overline{\overline{\mu}}. \end{aligned} \tag{10}$$

For this choice of $a$, in the limit as $\sigma$ tends to zero the uniaxial medium reduces to an isotropic space that is identical to the upper half-space.

The dispersion relationship is derived from (5) and is expressed as

$$k^2 = \frac{\beta_z^{a^2}}{\left(1 + \dfrac{\sigma}{j\omega\varepsilon_o}\right)^2} + \beta_x^{i^2} \tag{11}$$

which leads to

$$\beta_z^a = \pm \left(1 - j\frac{\sigma}{\omega\varepsilon_o}\right) \beta_z^i. \tag{12}$$

It is interesting to note that the real part of $\beta_z^a$ is identical to that of the incident wave, implying that the phase velocities are identical. The transverse characteristic wave impedance is also identical to the incident wave, resulting in the conclusion that the media are perfectly matched. Furthermore, the transmitted wave is also attenuating along the $z$ direction.

Finally, given a $TE_y$ incident wave, the field intensities in the uniaxial medium are given by

$$\vec{H}_2 = \hat{y} H_o e^{-j\beta_x^i x - j\beta_z^i z} e^{-\alpha_z z} \tag{13}$$

$$\vec{E}_2 = \left[ \hat{x} \frac{\beta_z^i}{\omega\varepsilon_o\varepsilon_r} - \hat{z} \frac{\beta_x^i \left(1 + \frac{\sigma}{j\omega\varepsilon_o}\right)}{\omega\varepsilon_o\varepsilon_r} \right] \cdot H_o e^{-j\beta_x^i x - j\beta_z^i z} e^{-\alpha_z z} \tag{14}$$

where

$$\alpha_z = \frac{\sigma}{\omega\varepsilon_o}\beta_z^i = \sigma\eta_o\sqrt{\varepsilon_r}\cos\theta^i \tag{15}$$

and $\theta^i$ is the angle of incidence relative to the $z$ axis. Thus, along the normal axis, the wave is propagating with the same phase velocity as the incident wave while simultaneously attenuating. Furthermore, the attenuation constant is independent of frequency, although it is dependent on the angle of incidence and the conductivity of the medium. It is observed that the propagation characteristic in (12) and the field solution (13) and (14) are identical to that derived using Berenger's method [2], [3] (note that in the notation used above $\sigma$ is normalized by $\epsilon_r$).

From (1)–(10), it is evident that any constant $a$ will satisfy the perfectly matched condition, and other choices of $a$ may have advantages. For example, it is observed in [13] and [14] that if $a = \kappa + \sigma/j\omega\varepsilon_o$, then if $\beta_z^i$ is complex from (12), $\gamma_z^a = -[\kappa\alpha_z^i + (\sigma/\omega\varepsilon_o)\beta_z^i] - j[\kappa\beta_z^i + (\sigma/\omega\varepsilon_o)\alpha_z^i]$. Subsequently, the real term $\kappa$ amplifies the attenuation of highly attenuative modes, and $\sigma$ attenuates the propagating modes. This was demonstrated numerically using the frequency domain finite-element method (FEM) [13], [14] and in the time domain using the FDTD [15].

## III. The Discrete Perfectly Matched Uniaxial Medium

The principal focus of this paper is implementing the uniaxial perfectly matched material medium within the FDTD algorithm. The FDTD method is based on the discrete representation of Maxwell's curl equations (Ampère's and Faraday's laws) [1]. In the uniaxial medium, Ampère's law is expressed in matrix form as

$$\begin{bmatrix} \frac{\partial}{\partial y}H_z - \frac{\partial}{\partial z}H_y \\ \frac{\partial}{\partial z}H_x - \frac{\partial}{\partial x}H_z \\ \frac{\partial}{\partial x}H_y - \frac{\partial}{\partial y}H_x \end{bmatrix} = j\omega\varepsilon_o\varepsilon_r \begin{bmatrix} 1 + \frac{\sigma}{j\omega\varepsilon_o} & 0 & 0 \\ 0 & 1 + \frac{\sigma}{j\omega\varepsilon_o} & 0 \\ 0 & 0 & \frac{1}{1 + \frac{\sigma}{j\omega\varepsilon_o}} \end{bmatrix} \begin{bmatrix} E_x \\ E_y \\ E_z \end{bmatrix}. \tag{16}$$

The first two rows of (16), corresponding to the transverse field components $E_x$ and $E_y$, are identical to the relationships encountered in a lossy isotropic medium. Subsequently, the time-dependent transverse field components can be computed via the standard explicit FDTD update expressions, e.g.,

$$E_{x_{i+1/2,j,k}}^{n+1/2} = \frac{2\varepsilon_o - \Delta t\sigma}{2\varepsilon_o + \Delta t\sigma} E_{x_{i+1/2,j,k}}^{n-1/2} + \frac{\frac{2\Delta t}{\varepsilon_r}}{2\varepsilon_o + \Delta t\sigma} \cdot \left( \frac{H_{z_{i+1/2,j+1/2,k}}^n - H_{z_{i+1/2,j-1/2,k}}^n}{\Delta y} - \frac{H_{y_{i+1/2,j,k+1/2}}^n - H_{y_{i+1/2,j,k-1/2}}^n}{\Delta z} \right). \tag{17}$$

However, $E_z$ cannot be updated in this manner due to the nonlinear frequency dependence of $\epsilon_{zz}$. In fact, observing (16) it is seen that $\epsilon_{zz}$ is dispersive and has a positive imaginary term which implies a negative conductivity along the $z$ axis.

$E_z$ can be updated in any number of ways. However, a two-step method based on a difference equation is found to be the most efficient. To this end, the normal electric flux density is introduced as

$$D_z = \frac{\varepsilon_o\varepsilon_r}{1 + \frac{\sigma}{j\omega\varepsilon_o}} E_z. \tag{18}$$

The third row of (16) is then expressed in the time domain as $(\partial/\partial x)H_y - (\partial/\partial y)H_x = (\partial/\partial t)D_z$. $D_z$ is then updated using the standard FDTD formulation

$$D_{z_{i,j,k+1/2}}^{n+1/2} = D_{z_{i,j,k+1/2}}^{n-1/2} + \Delta t \cdot \left( \frac{H_{y_{i+1/2,j,k+1/2}}^n - H_{y_{i-1/2,j,k+1/2}}^n}{\Delta x} - \frac{H_{x_{i,j+1/2,k+1/2}}^n - H_{x_{i,j-1/2,k+1/2}}^n}{\Delta y} \right). \tag{19}$$

From (18), $E_z$ can be calculated from $D_z$. Specifically

$$\left(1 + \frac{\sigma}{j\omega\varepsilon_o}\right) D_z = \varepsilon_o\varepsilon_r E_z$$

or

$$j\omega D_z + \frac{\sigma}{\varepsilon_o} D_z = j\omega\varepsilon_o\varepsilon_r E_z. \tag{20}$$

This is then transformed into the time domain using a Fourier transform where $j\omega \to \partial/\partial t$. Approximating the time derivatives using a central difference approximation and averaging $(\sigma/\varepsilon_o)\, D_z$ in time; this results in the difference equation that is second-order accurate

$$E_z^{n+1/2} = E_z^{n-1/2} + \frac{1}{\varepsilon_o\varepsilon_r} \cdot \left[ D_z^{n+1/2}\left(1 + \frac{\sigma\Delta t}{2\varepsilon_o}\right) - D_z^{n-1/2}\left(1 - \frac{\sigma\Delta t}{2\varepsilon_o}\right) \right]. \tag{21}$$

Then, (19) and (21) can be used to update the normal electric-field component. It is observed that this two-step update does require additional storage since the previous time history of both $D_z$ and $E_z$ must be known. Dual expressions are similarly derived for the magnetic field updates, again, using a two-step scheme to update $H_z$ and standard FDTD update expressions for the transverse field components. Finally, the explicit solu-

tion procedure is stable within the Courant stability limit that is used for the traditional FDTD method [1].

The previous analysis assumed that the PML interface is a constant $z$ plane. For planes in constant $x$ and $z$ planes the uniaxial parameters are simply permuted and similar update expressions can easily be derived.

This perfectly matched material medium can also be applied to inhomogeneous media as well, such as the analysis of printed circuits or antennas within layered substrates/superstrates. Lossy and dispersive dielectrics can also be modeled by introducing a complex $\epsilon_r$ in (16) and deriving the appropriate expressions [15].

## IV. Relationship with Berenger's PML

It is interesting that the propagation characteristics of the transmitted wave of the uniaxial PML medium are identical to that of Berenger's PML medium [2]–[4]. This implies that there is a physical equivalence between the two media. However, a mathematical relationship between the two methods is not obvious. The objective of this section is to derive this relationship. To this end, we will begin with Berenger's PML method and then proceed to manipulate it into a form that is equivalent to the uniaxial PML in (16).

Berenger's equations in three dimensions can be found in [4]. Here, we start with the modified Ampère's law expressed in the frequency domain

$$j\omega\varepsilon_o\varepsilon_r\left(1+\frac{\sigma_y}{j\omega\varepsilon_o\varepsilon_r}\right)E_{xy}=\frac{\partial}{\partial y}(H_{zx}+H_{zy}) \tag{22a}$$

$$j\omega\varepsilon_o\varepsilon_r\left(1+\frac{\sigma_z}{j\omega\varepsilon_o\varepsilon_r}\right)E_{xz}=-\frac{\partial}{\partial z}(H_{yx}+H_{yz}) \tag{22b}$$

$$j\omega\varepsilon_o\varepsilon_r\left(1+\frac{\sigma_z}{j\omega\varepsilon_o\varepsilon_r}\right)E_{yz}=\frac{\partial}{\partial z}(H_{xy}+H_{xz}) \tag{22c}$$

$$j\omega\varepsilon_o\varepsilon_r\left(1+\frac{\sigma_x}{j\omega\varepsilon_o\varepsilon_r}\right)E_{yx}=-\frac{\partial}{\partial x}(H_{zx}+H_{zy}) \tag{22d}$$

$$j\omega\varepsilon_o\varepsilon_r\left(1+\frac{\sigma_x}{j\omega\varepsilon_o\varepsilon_r}\right)E_{zx}=\frac{\partial}{\partial x}(H_{yx}+H_{yz}) \tag{22e}$$

$$j\omega\varepsilon_o\varepsilon_r\left(1+\frac{\sigma_y}{j\omega\varepsilon_o\varepsilon_r}\right)E_{zy}=-\frac{\partial}{\partial y}(H_{xy}+H_{xz}). \tag{22f}$$

As in Section II, it is assumed that the interface between the PML media and the isotropic space is a constant $z$ plane. Subsequently, let $\sigma_x = \sigma_y = 0$ and $\sigma = \sigma_z/\epsilon_r$. Then, adding (22a) with (22b), (22c) with (22d), and (22e) with (22f), and using the relationship that $E_x = E_{xy} + E_{xz}$, $E_y = E_{yx} + E_{yz}$, $E_z = E_{zx} + E_{zy}$, and similarly for the magnetic field intensities leads to

$$j\omega\varepsilon_o\varepsilon_r E_x=\frac{\partial}{\partial y}H_z-\frac{\dfrac{\partial}{\partial z}H_y}{1+\dfrac{\sigma}{j\omega\varepsilon_o}} \tag{23a}$$

$$j\omega\varepsilon_o\varepsilon_r E_y=\frac{\dfrac{\partial}{\partial z}H_x}{1+\dfrac{\sigma}{j\omega\varepsilon_o}}-\frac{\partial}{\partial x}H_z \tag{23b}$$

$$j\omega\varepsilon_o\varepsilon_r E_z=\frac{\partial}{\partial x}H_y-\frac{\partial}{\partial y}H_x. \tag{23c}$$

This procedure is repeated for the modified Faraday's law leading to

$$-j\omega\mu_o\mu_r H_x=\frac{\partial}{\partial y}E_z-\frac{\dfrac{\partial}{\partial z}E_y}{1+\dfrac{\sigma}{j\omega\varepsilon_o}} \tag{24a}$$

$$-j\omega\mu_o\mu_r H_y=\frac{\dfrac{\partial}{\partial z}E_x}{1+\dfrac{\sigma}{j\omega\varepsilon_o}}-\frac{\partial}{\partial x}E_z \tag{24b}$$

$$-j\omega\mu_o\mu_r H_z=\frac{\partial}{\partial x}E_y-\frac{\partial}{\partial y}E_x. \tag{24c}$$

The sets of equations in (23a)–(c) and (24a)–(c) are identical to those derived by Rappaport [16] via a coordinate stretching method. That is, starting from Maxwell's curl equations, the normal coordinate $z$ is mapped into the stretched space with the complex spatial variable

$$z=z'\left(1+\frac{\sigma}{j\omega\varepsilon_o}\right) \tag{25}$$

and subsequently leading to (23a)–(c) and (24a)–(c).

Comparing (23a)–(c) and (24a)–(c) with the uniaxial medium in (16) implies that there is a scaling of the normal electric and magnetic fields where

$$E_z=\frac{E_z'}{1+\dfrac{\sigma}{j\omega\varepsilon_o}} \tag{26a}$$

$$H_z=\frac{H_z'}{1+\dfrac{\sigma}{j\omega\varepsilon_o}}. \tag{26b}$$

(Alternatively, a scaling of the transverse fields could have been used.) Applying the field transformations to (23a)–(c) and (24a)–(c) and then multiplying (23a), (23b), (24a), and (24b) by $(1+\sigma/j\omega\varepsilon_o)$ leads to

$$j\omega\varepsilon_o\varepsilon_r E_x\left(1+\frac{\sigma}{j\omega\varepsilon_o}\right)=\frac{\partial}{\partial y}H_z'-\frac{\partial}{\partial z'}H_y \tag{27a}$$

$$j\omega\varepsilon_o\varepsilon_r E_y\left(1+\frac{\sigma}{j\omega\varepsilon_o}\right)=\frac{\partial}{\partial z'}H_x-\frac{\partial}{\partial x}H_z' \tag{27b}$$

$$\frac{j\omega\varepsilon_o\varepsilon_r E_z'}{1+\dfrac{\sigma}{j\omega\varepsilon_o}}=\frac{\partial}{\partial x}H_y-\frac{\partial}{\partial y}H_x \tag{27c}$$

$$-j\omega\mu_o\mu_r H_x\left(1+\frac{\sigma}{j\omega\varepsilon_o}\right)=\frac{\partial}{\partial y}E_z'-\frac{\partial}{\partial z'}E_y \tag{28a}$$

$$-j\omega\mu_o\mu_r H_y\left(1+\frac{\sigma}{j\omega\varepsilon_o}\right)=\frac{\partial}{\partial z'}E_x-\frac{\partial}{\partial x}E_z' \tag{28b}$$

$$-\frac{j\omega\mu_o\mu_r H_z'}{1+\dfrac{\sigma}{j\omega\varepsilon_o}}=\frac{\partial}{\partial x}E_y-\frac{\partial}{\partial y}E_x. \tag{28c}$$

Equations (27a)–(c) are identical to (16) and similarly for the dual equations in (28a)–(c). Thus, Berenger's formulation can be derived from the uniaxial PML formulation (and vice versa) through a scaling of the normal field intensities. Furthermore, since the fields satisfying (27a)–(c) and (28a)–(c) have identical propagation characteristics as those described

by Berenger's modified Maxwell's equations, a mathematical equivalence between the two formulations can be drawn.

## V. Corner Regions

The previous analysis only considers the case of a wave incident on a single planar boundary. However, for unbounded problems the FDTD lattice must be terminated by PML on all six sides. An ambiguity occurs in the corner regions where there is more than one normal interface boundary. Within these regions, a more generalized constitutive relationship is necessary. In this region, Maxwell's curl equations are expressed as

$$\begin{aligned} \nabla \times \vec{H} &= j\omega\varepsilon_o\varepsilon_r\overline{\overline{\varepsilon}}\vec{E} \\ \nabla \times \vec{E} &= -j\omega\mu_o\overline{\overline{\mu}}\vec{H} \end{aligned} \tag{29}$$

where

$$\overline{\overline{\varepsilon}} = \overline{\overline{\mu}} = \begin{bmatrix} \dfrac{s_y s_z}{s_x} & 0 & 0 \\ 0 & \dfrac{s_x s_z}{s_y} & 0 \\ 0 & 0 & \dfrac{s_x s_y}{s_z} \end{bmatrix} \tag{30}$$

and

$$\begin{aligned} s_x &= 1 + \frac{\sigma_x}{j\omega\varepsilon_o} \\ s_y &= 1 + \frac{\sigma_y}{j\omega\varepsilon_o} \\ s_z &= 1 + \frac{\sigma_z}{j\omega\varepsilon_o}. \end{aligned} \tag{31}$$

It is noted that $s_x$, $s_y$, and $s_z$ are associated with the $x$, $y$, and $z$-normal planes, respectively. Outside of these regions, the respective $\sigma_i = 0$. Furthermore, it will be noted in Section VI that $s_x$, $s_y$, and $s_z$ are only spatially variant along the $x$, $y$, and $z$ directions, respectively. However, they must be invariant along their transverse directions. It is also noted that Berenger's equations can again be derived directly from (29)–(31) by normalizing the fields $E_i' = E_i/s_i$, $(i = x, y, z)$, and performing a field splitting.

In the corner regions, the time-dependent fields are updated within the FDTD algorithm by using similar techniques as the updates associated with the normal field components presented in Section III. As an example, consider the update of $E_z$ from Ampere's law. We introduce the definition of the flux density as

$$D_z = \varepsilon_o\varepsilon_r \frac{s_x}{s_z} E_z. \tag{32}$$

Then, from (29) and (30)

$$\begin{aligned} \frac{\partial}{\partial x} H_y - \frac{\partial}{\partial y} H_x &= j\omega s_y D_z \\ &= j\omega D_z + \frac{\sigma_y}{\varepsilon_o} D_z. \end{aligned} \tag{33}$$

Transforming this into the time domain, $D_z$ is then updated using a standard explicit FDTD expression similar to (17). From (32), $E_z$ can be calculated from $D_z$. Specifically,

$$s_z D_z = \varepsilon_o\varepsilon_r s_x E_z$$

or

$$j\omega D_z + \frac{\sigma_z}{\varepsilon_o} D_z = \varepsilon_o\varepsilon_r \left( j\omega E_z + \frac{\sigma_x}{\varepsilon_o} E_z \right). \tag{34}$$

Transforming this into the time-domain, approximating the time derivatives using a central difference approximation, and averaging $(\sigma_z/\varepsilon_o)D_z$ and $(\sigma_x/\varepsilon_o)E_z$ in time results in the following second-order accurate explicit update:

$$\begin{aligned} E_z^{n+1/2} = E_z^{n-1/2} & \frac{1 - \dfrac{\sigma_x \Delta t}{2\varepsilon_o}}{1 + \dfrac{\sigma_x \Delta t}{2\varepsilon_o}} + \frac{1}{\left(1 + \dfrac{\sigma_x \Delta t}{2\varepsilon_o}\right)\varepsilon_o\varepsilon_r} \\ & \cdot \left[ D_z^{n+1/2} \left( 1 + \frac{\sigma_z \Delta t}{2\varepsilon_o} \right) - D_z^{n-1/2} \left( 1 - \frac{\sigma_z \Delta t}{2\varepsilon_o} \right) \right]. \end{aligned} \tag{35}$$

Subsequently, this results in an explicit update that is second-order accurate and stable within the Courant limit of the interior FDTD space.

## VI. Numerical Results

The perfectly matched medium described in the Sections II and III has been applied to the truncation of FDTD lattices for the application of printed circuit devices. The uniaxial medium is thus placed at the outer extremities of the mesh. Conceptually, this emulates an anechoic chamber in which the interior isotropic solution space is the working volume and the uniaxial perfectly matched medium is the absorbing material. Within the working volume, the electric and magnetic fields are updated using the traditional FDTD solution [1]. This is highly computationally efficient and can be performed using means such as those described in [17]. Within the absorbing region, the transverse field components are also updated using the traditional FDTD update expressions, whereas the normal field components are updated using the two-step approach presented in Section III.

As an illustrative example, the uniaxial PML medium was used to terminate an FDTD grid for the simulation of a Gaussian pulse excitation of a shielded microstrip line (Fig. 1). The shielded strip line is printed on a dielectric substrate with $\epsilon_r = 2.2$. The microstrip line is shielded so as to study the terminating effects of the endwall only. Berenger found that if $\sigma$ is constant throughout the PML media (specifically with respect to the $z$ axis) significant reflections are encountered at the interface of the PML [2]. This is due to the discrete approximation of the fields and the material parameters at the interface of the two media which results in a spurious impedance loading at the interface. This mismatch problem in the discrete space can be tempered by using a spatially varying conductivity, as suggested in [2]. Specifically, $\sigma$ is chosen to be spatially variant along the normal axis as

$$\sigma(z) = \frac{\sigma_{\max} |z - z_o|^m}{d^m} \tag{36}$$

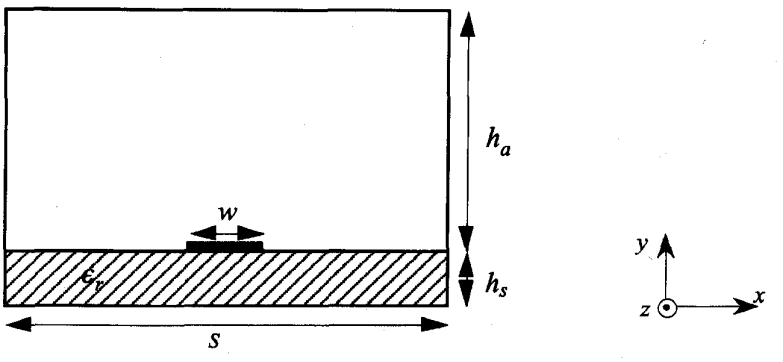


Fig. 1. Cross section of uniform shielded microstrip line for study of reflection properties of PML boundary condition. ($w = 0.254$ mm, $h_s = 0.254$ mm, $h_a = 0.762$ mm, $S = 2.11$ mm, $\epsilon_r = 2.2$, $\Delta x = \Delta y = 0.0423333$ mm, $\Delta z = 0.12$ mm.) The end walls (normal to the $z$ direction) are terminated into a uniaxial PML slab.

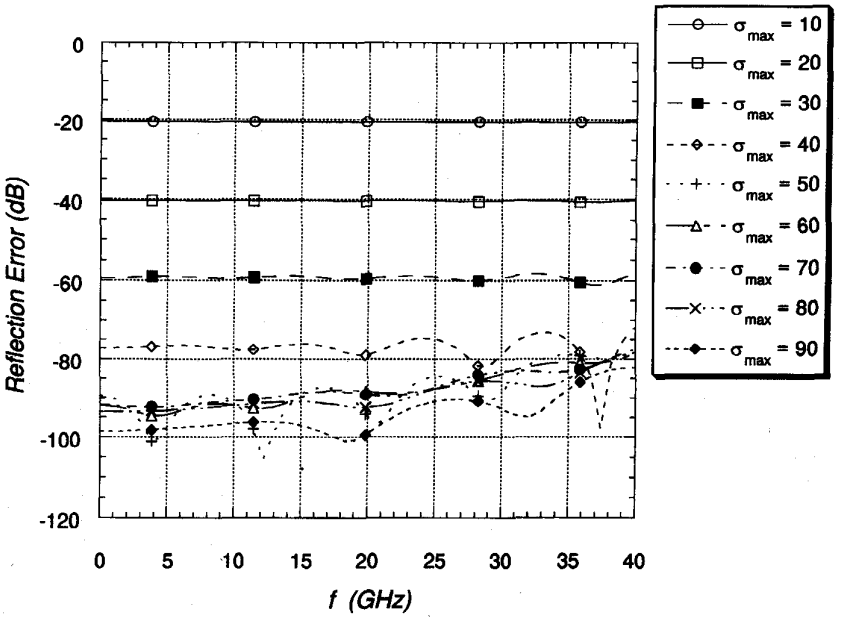


Fig. 2. Reflection error due to a ten-cell thick PML termination of the strip line circuit (e.g., along the $z$ axis) for various values of $\sigma_{\max}$ ($m = 4$).

where $z_o$ is the interface, $d$ is the depth of the PML, and $m$ is order of the polynomial variation. This helps to smooth the transition into the PML medium and, consequently, smaller reflections are encountered.

The PML is backed by a PEC wall; thus, from (15) the expectant reflection error is expected to be [3], [4]

$$R_m(\theta^i) = e^{-2\eta_o\sqrt{\epsilon_r}\sigma_{\max}d\,\cos\,\theta^i/(m+1)}. \tag{37}$$

One then expects that by increasing $\sigma$ the reflection error will continuously reduce. However, it is demonstrated below that due to discretization error and numerical rounding error, there is a lower bound on the realizable reflection in the discrete space.

The reflection error versus frequency due to a ten cell PML termination of the FDTD lattice modeling the strip line structure is illustrated in Fig. 2 for various values of $\sigma_{\max}$. The strip line was excited by a voltage source with a Gaussian profile and a 50 GHz bandwidth. For this case, the spatial variation of the conductivity was fourth order ($m = 4$). As expected, the reflection error is quite flat versus frequency for small values of $\sigma_{\max}$. Fig. 3 compares the computed reflection error at DC [$\Gamma_4$(PML)] versus $R_4(0)$, as predicted by (37). The predicted value from (37) assumes the relative permittivity to be the effective permittivity of the strip line $\epsilon_{reff} = 1.76$. For small values of $\sigma$, the reflection error is predicted quite well. However, as $\sigma$ increases the reflection, error levels off due to discretization and rounding errors. It was also found that if $\sigma$ is increased further, the reflection error will eventually increase due to discretization error.

The previous results were compared to those simulated using Berenger's method (an example is illustrated in Fig. 4). Remarkably, the solutions are equivalent within four to five digits. Based on the analysis in Section IV, this should not be surprising. However, since the update expressions are quite different than Berenger's equations, some deviation was expected. It is also noted that the uniaxial PML computation required 30 seconds and the Berenger PML required 48

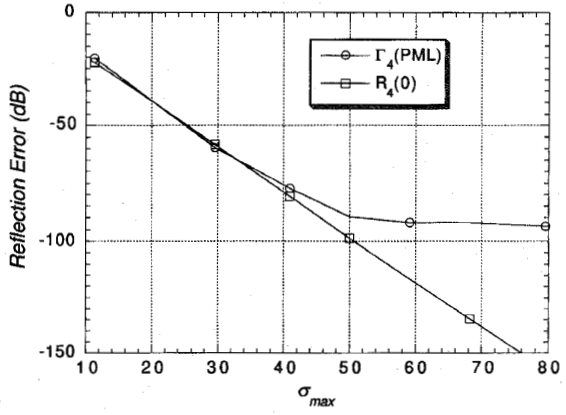


Fig. 3. Comparison of the reflection error at dc ($f = 0$) due to a ten-cell thick PML termination of the strip line ($m = 4$) computed using the uniaxial PML method compared with the reflection error predicted by (37) ($\Delta z = 0.12$ mm and $\epsilon_{reff} = 1.76$).

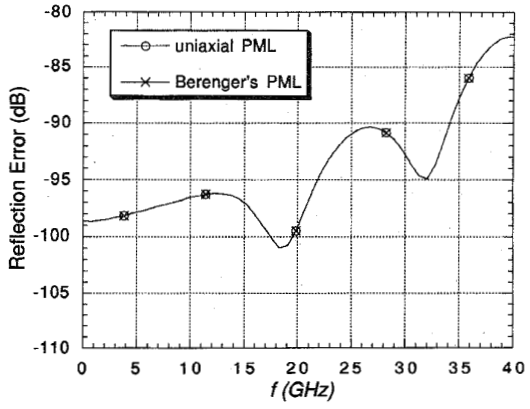


Fig. 4. Comparison of the reflection error due to a ten-cell thick PML termination of the strip line with $\sigma_{\max} = 90$ and $m = 4$ encountered using the uniaxial PML method and Berenger's PML method.

seconds on a single processor Cray Y-MP to perform 2100 iterations on a 51 × 51 × 25 grid.

A second example is that of a simple microstrip structure. To this end, the effective termination of a 50-Ω microstrip line (10-mil width, zero thickness) printed on a 10-mil Alumina substrate ($\epsilon_r = 9.8$) is studied. The discrete model was based on a uniform mesh with $\Delta x = \Delta y = 0.042\,333$ mm, $\Delta z = 0.12$ mm, and $\Delta t = 0.085$ ps. The microstrip line was excited by a voltage source with a Gaussian profile and a 40 GHz bandwidth. The uniaxial PML was used to terminate all boundaries, with exception to the ground plane, and the corner condition presented in Section V was implemented. A number of studies were performed with this structure to characterize the effects of the depth and conductivity of the PML and the order of spatial variation $m$ on the absorbing properties of the PML medium. Initially, the depth is set to ten cells and $m$ to four. The reflection error due to the PML boundary which the microstrip line terminates into ($z$ normal) is illustrated in Fig. 5 for various values of $\sigma_{\max}$. Fig. 6 illustrates the reflection error due to this same boundary as a function of $m$, again for a ten-cell thick PML. For each case, $\sigma_{\max}$ is chosen to yield the minimum reflection error. It appears that $m = 4$ provides the smallest reflection error over the frequency band illustrated. In fact, for most of the cases that have been studied thus far, $m = 4$ has minimized the reflection error.

In all cases that have been studied, it has been observed that there is an optimal value for $\sigma_{\max}$ which the minimizes reflection error. For example, in Fig. 5 this appears to occur in the region of $40 \leq \sigma_{\max} \leq 60$. This becomes more apparent by comparing the computed reflection error with the error predicted by (37). This is provided in Fig. 7 both for a ten-cell PML layer for $m = 2$ and 4, and for a five-cell PML layer for $m = 4$. The relative permittivity used in (37) is chosen to be the effective permittivity ($\epsilon_{reff} = 6.62$) of the 50-Ω microstrip line. As seen for the strip-line example, the comparison is quite good for smaller values of $\sigma_{\max}$ and then levels off. It is interesting to note that for the ten-cell PML it has been observed fairly consistently that the minimum reflection error occurs when $R_m(0) \approx e^{-16}$, whereas for the five-cell PML, the minimum reflection error occurs when $R_m(0) \approx e^{-8}$. From this trend, a choice for $\sigma_{\max}$ that will minimize reflection is expressed as

$$\sigma_{\max} \approx \frac{(m+1)}{150\pi\Delta\sqrt{\varepsilon_r}} \tag{38}$$

where $\Delta$ is the spatial discretization (in meters) along the normal axis of the PML layer, $m$ is the order of the polynomial in (36), and $\epsilon_r$ is the effective relative permittivity for the inhomogeneous medium. When $\sigma_{\max}$ is less than this value, the reflection error is dominated by reflection from the back PEC wall. When $\sigma_{\max}$ is greater than this value, discretization error dominate and will ultimately increase as $\sigma_{\max}$ grows much larger.

The previous examples concentrated mainly on the end-wall termination into which the microstrip line is terminating. It is also important to do a study of the side-wall reflections which have highly oblique waves and surface-wave modes incident upon them. In Fig. 8, the reflection error encountered due to the side wall reflections is illustrated for a ten-cell PML medium ($m = 4$) and for various distances between the PML interface and the edge of the microstrip. As expected, the reflection error is larger than the end-wall termination reflections. It is seen that if less than $-70$ dB reflection is encountered across the band, the interface must be at least seven cells from the edge of the microstrip. Interestingly, from numerical experimentation, it has been found that as $\epsilon_r$ decreases the interface can be placed closer to the strip edge (for $\epsilon_r = 2.2$, three cells from the strip edge was sufficient). It is suspected that this phenomena is due to the increased levels of surface-wave mode power as $\epsilon_r$ increases—although this is a topic for further research.

The final example is the analysis of a printed antenna using the FDTD and the uniaxial PML boundary condition. The geometry of the patch antenna that was simulated is superimposed in the graph in Fig. 9. Simulated results using the FDTD algorithm and measured results for this antenna were published in [18] and [19]. The discretization used for this problem was $\Delta x = 0.389$ mm, $\Delta y = 0.4$ mm,

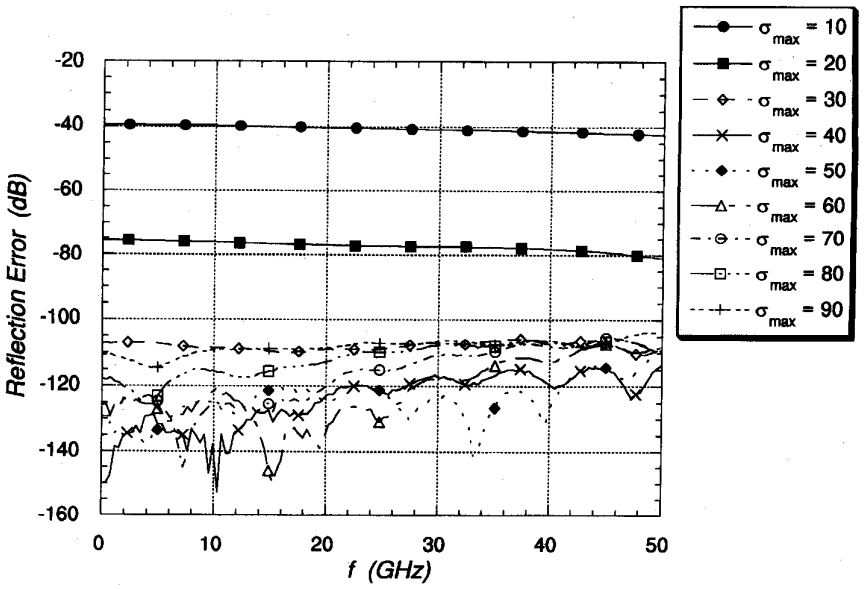


Fig. 5. Reflection error due to a ten-cell thick uniaxial PML termination of the 50-Ω microstrip line ($m = 4$) for various values of $\sigma_{\max}$. (10-mil strip width, 10-mil Alumina substrate with $\epsilon_r = 9.8$).

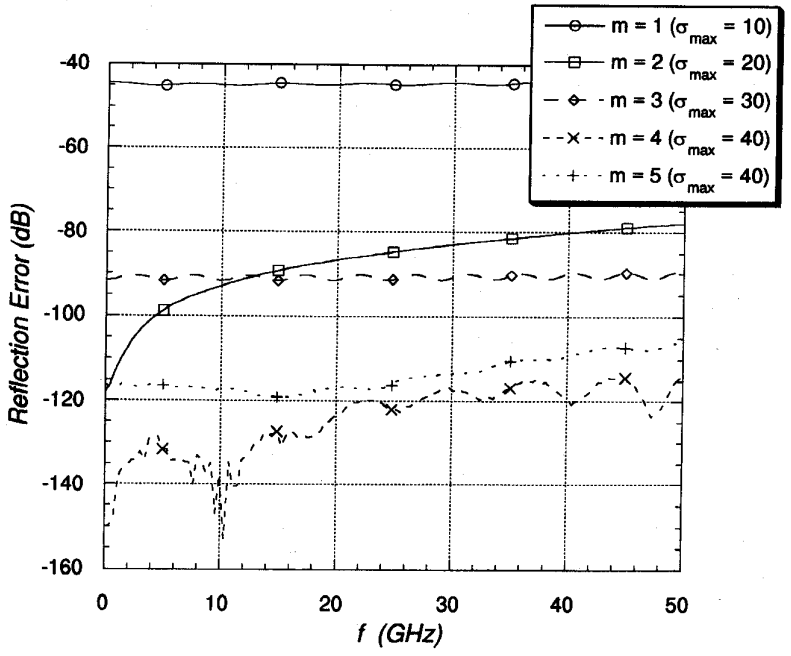


Fig. 6. Reflection error due to a ten-cell thick uniaxial PML termination of the 50-Ω microstrip line for various values of $m$. The value of $\sigma_{\max}$ is chosen for the minimum reflection error in each case.

$\Delta z = 0.1588$ mm, and $\Delta t = 0.441$ ps. The source microstrip line was 50 cells long and was excited by a voltage source with a Gaussian profile and a 30-GHz bandwidth. The interfaces of the PML media were placed three cells from the edge of the patch antenna, and five cells above the surface of the antenna. The PML slabs were ten-cells thick. Fig. 9 compares the reflection loss $|S_{11}|$ computed using the FDTD and the PML boundary that was positioned as described above with the case when the PML boundaries were placed much further away. Negligible difference is observed in the result.

## VII. Summary

A new perfectly matched layer (PML) absorbing material composed of a uniaxial anisotropic material for the truncation of FDTD lattices has been presented. It was shown that by properly choosing the constitutive parameters, a lossy uniaxial

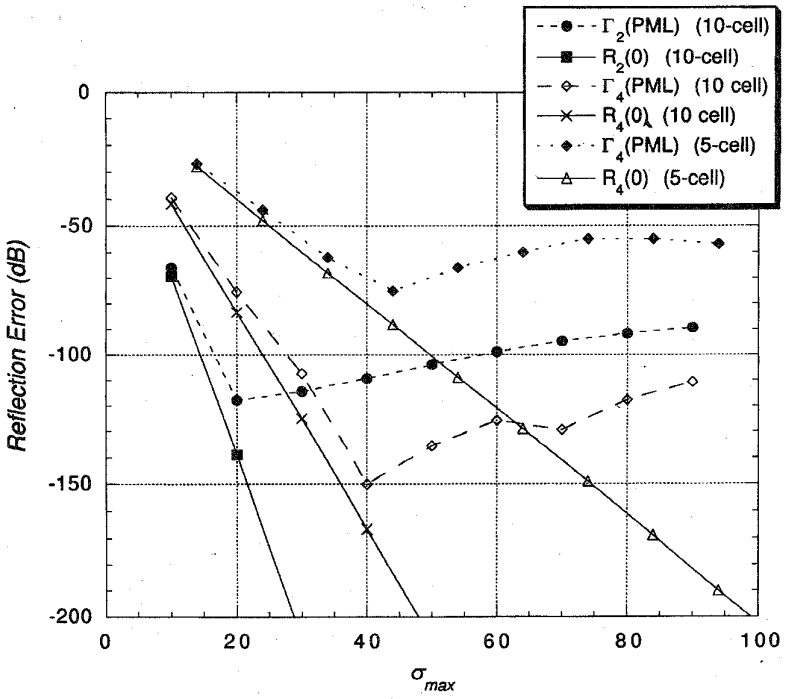


Fig. 7. Comparison of the reflection error at dc ($f = 0$) computed using the uniaxial PML method compared with the reflection error predicted by (37) due to a ten-cell thick PML termination of the microstrip line for $m = 4$ and $m = 2$, and due to a five-cell thick PML termination of the microstrip line for $m = 4$ ($\Delta z = 0.12$ mm and $\epsilon_{reff} = 6.62$).

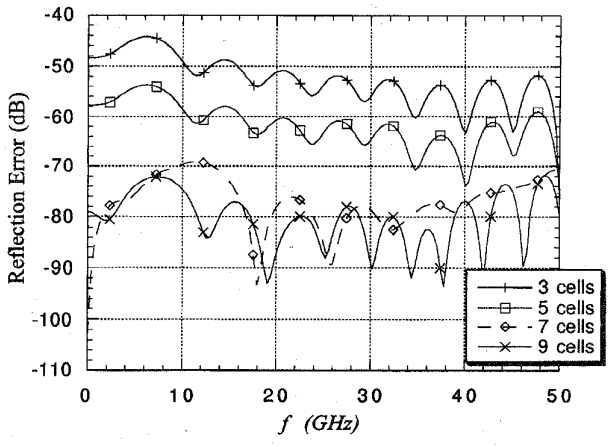


Fig. 8. Reflection error due to a ten-cell thick uniaxial PML termination of the side walls for a 50-Ω microstrip line as the distance from the edge of the strip from the PML interfaced is increased from three to nine cells.

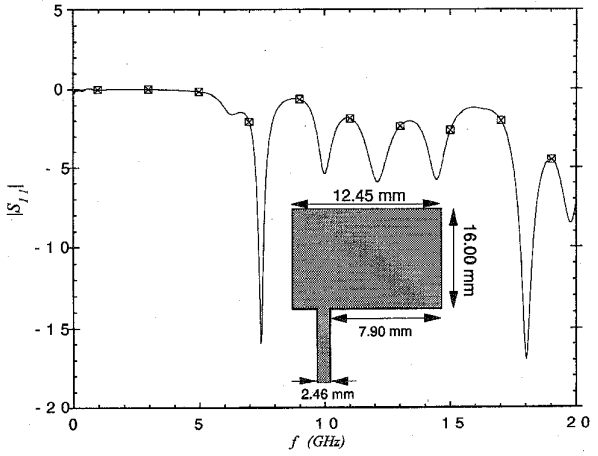


Fig. 9. $|S_{11}|$ of a microstrip fed-patch antenna (superimposed) printed on a 31.25 mil Duroid substrate ($\epsilon_r = 2.2$) computed via the FDTD method. The FDTD lattice is terminated by a 10-cell thick uniaxial PML layer which is placed — × — three cells from the edge of the patch, five cells above the patch, and —□— ten cells from the edges of the patch.

media can be perfectly matched to an isotropic space. Unlike Berenger's technique, the PML absorbing media presented in this paper is based on a Maxwellian formulation. However, a mathematical equivalence between the two methods was demonstrated. The lossy uniaxial PML medium offers a number of significant advantages over previously derived formulations. Foremost, it is based on Maxwell's equations, rather than a modified set of equations. Thus, it can easily be applied to other techniques, such as finite-element methods or nonorthogonal FDTD methods based on unstructured grids, such as the generalized Yee algorithm [1], that are based on non-Cartesian meshes. It also provides the satisfaction that perhaps a physical uniaxial material could be constructed with such broad-band absorbing characteristics. The challenge presented by such a concept is that one must be able to construct a material that exhibits simultaneously the electric and magnetic properties of (16) over a broad frequency range.

Numerical examples demonstrated that the FDTD implementation of the uniaxial PML medium is stable, and equivalent in effectiveness as compared to Berenger's PML medium.

It was also demonstrated that the current method is more computationally efficient than Berenger's technique, making it more attractive.

Finally, the formulation in Section II was presented in a general manner, in that any nonzero value of $a$ results in a matched condition. Perhaps there is a more advantageous choice for the constitutive parameter $a$ than $1 + \sigma/j\omega\varepsilon_o$ or $\kappa + \sigma/j\omega\varepsilon_o$ that would benefit the numerical simulation or the physical absorber. This is the subject of further investigation.

## REFERENCES


[1] A. Taflove, Ed., *Finite Difference Time Domain Methods for Electrodynamic Analyses.* NY: Artech House, May 1995.

[2] J.-P. Berenger, "A perfectly matched layer for the absorption of electromagnetic waves," *J. Computat. Phys.,* Oct. 1994.

[3] W. C. Chew and W. H. Weedon, "A 3-D perfectly matched medium from modified Maxwell's equations with stretched coordinates," *Microwave Opt. Tech. Lett.,* vol. 7, pp. 599–604, Sept. 1994.

[4] D. S. Katz, E. T. Thiele, and A. Taflove, "Validation and extension to three-dimensions of the Berenger PML absorbing boundary condition for FDTD meshes," *IEEE Microwave Guided Wave Lett.,* vol. 4, pp. 268–270, Aug. 1994.

[5] C. E. Reuter, R. M. Joseph, E. T. Thiele, D. S. Katz, and A. Taflove, "Ultrawideband absorbing boundary condition for termination of waveguiding structures in FDTD simulations," *IEEE Microwave Guided Wave Lett.,* vol. 4, pp. 344–346, Apr. 1994.

[6] R. Mittra and Ü. Pekel, "A new look at the perfectly matched layer (PML) concept for the reflectionless absorption of electromagnetic waves," *IEEE Microwave Guided Wave Lett.,* vol. 5, pp. 84–87, Mar. 1995.

[7] S. D. Gedney and A. Roden, "Applying Berenger's perfectly matched layer (PML) boundary condition to nonorthogonal FDTD analyzes of planar microwave circuits," in *URSI Radio Sci. Meet. Dig.,* Newport Beach, CA, June 18–23, 1995, p. 334.

[8] E. A. Navarro, C. Wu, P. Y. Chung, and J. Litva, "Application of PML superabsorbing boundary condition to nonorthogonal FDTD method," *Elec. Lett.,* vol. 30, no. 20, pp. 1654–1656, 1994.

[9] W. Chen, E. A. Navarro, P. Y. Chung, and J. Litva, "Modeling of waveguide structures using the nonorthogonal FDTD method with a PML absorbing boundary," *Microwave Opt. Tech. Lett.,* vol. 8, no. 4, pp. 226–228, Mar. 1995.

[10] S. Gedney and U. Navsariwala, "An unconditionally stable implicit finite-element time-domain solution of the vector wave equation," *IEEE Microwave Guided Wave Lett.,* vol. 5, pp. 332–334, Oct. 1995.

[11] J.-F. Lee and Z. Sacks, "Whitney elements time-domain method (WETD)," *IEEE Trans. Magn.,* vol. 31, pp. 1325–1329, May 1995.

[12] S. D. Gedney and F. Lansing, "A parallel planar generalized Yee-algorithm for the analysis of microwave circuit devices," *Int. J. Numerical Modeling (Electron. Networks, Devices, Fields),* vol. 8, pp. 249–264, May–Aug. 1995.

[13] D. Kingsland, R. Dycziz-Edlinger, J. F. Lee, and R. Lee, "Performance characterization of a perfectly matched anisotropic absorber for frequency domain FEM applications," in *URSI Symp. Dig.,* Newport Beach, CA, June 1995, p. 339.

[14] Z. S. Sacks, D. M. Kingsland, R. Lee, and J. F. Lee, "A perfectly matched anisotropic absorber for use as an absorbing boundary condition," *IEEE Trans. Antennas Propagat.* vol. 43, pp. 1460–1463, Dec. 1995.

[15] S. D. Gedney, "An anisotropic PML absorbing media for FDTD simulation of fields in lossy dispersive media," *Electromagn.,* vol. 16, no. 3, pp. 339–416, July/Aug. 1996.

[16] C. M. Rappaport, "Perfectly matched absorbing boundary conditions based on anisotropic lossy mapping of space," *IEEE Microwave Guided Wave Lett.,* vol. 5, pp. 90–92, Mar. 1995.

[17] S. D. Gedney, "Finite-difference time-domain analysis of microwave circuit devices on high performance vector/parallel computers," *IEEE Trans. Microwave Theory Tech.,* vol. 43, pp. 2510–2514, Oct. 1995.

[18] D. M. Sheen, S. M. Ali, M. D. Abouzahra, and J. A. Kong, "Application of the three-dimensional finite-difference time-domain method to the analysis of planar microstrip circuits," *IEEE Trans. Antennas Propagat.,* vol. 38, pp. 849–857, July 1990.

[19] A. Tulintseff, "The finite-difference time-domain method and computer program description applied to multilayered microstrip antenna and circuit configurations," Jet Propulsion Lab., Pasadena, CA, AMT: 336.5-92-041, Tech. Rep., May 1992.


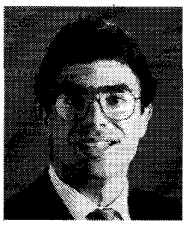


**Stephen D. Gedney** (S'84–M'91) received the B.Eng.-Honors degree from McGill University, Montreal, P.Q., Canada, in 1985, and the M.S. and Ph.D. degrees in electrical engineering from the University of Illinois, Urbana-Champaign, IL, in 1987 and 1991, respectively.

From 1985 to 1987, he worked for the U.S. Army Corps of Engineers, Champaign, IL, where he was engaged in research in electromagnetic pulse (EMP) simulation and propagation. Since 1991, he has been an Assistant Professor of Electrical Engineering at the University of Kentucky. In 1992 and 1993, he received the NASA/ASEE Summer Faculty Fellowship through the Jet Propulsion Laboratory, Pasadena, CA, where he was involved in the development of techniques for the full-wave analysis of printed microwave circuits and antennas. His current area of research is in the field of computational electromagnetics with a specific emphasis on the development of numerical solutions of the time-dependent Maxwell's equations for the rigorous analysis of microwave circuits and antennas, electrical interconnects of VLSI packages, and electromagnetic scattering, as well as the development of highly scalable algorithms for high performance parallel computers to apply these techniques to the analysis of large scale problems.

Dr. Gedney received the NSF Research Initiation award in 1993 and the NSF CAREER Award in 1996.